



Since January 2020 Elsevier has created a COVID-19 resource centre with free information in English and Mandarin on the novel coronavirus COVID-19. The COVID-19 resource centre is hosted on Elsevier Connect, the company's public news and information website.

Elsevier hereby grants permission to make all its COVID-19-related research that is available on the COVID-19 resource centre - including this research content - immediately available in PubMed Central and other publicly funded repositories, such as the WHO COVID database with rights for unrestricted research re-use and analyses in any form or by any means with acknowledgement of the original source. These permissions are granted for free by Elsevier for as long as the COVID-19 resource centre remains active.



Peritoneal M2 macrophage-derived extracellular vesicles as natural multitarget nanotherapeutics to attenuate cytokine storms after severe infections

Yizhuo Wang^a, Shuyun Liu^a, Lan Li^a, Ling Li^b, Xueli Zhou^b, Meihua Wan^c, Peng Lou^a, Meng Zhao^a, Ke Lv^a, Yujia Yuan^a, Younan Chen^a, Yanrong Lu^a, Jingqiu Cheng^a, Jingping Liu^{a,*}

^a NHC Key Laboratory of Transplant Engineering and Immunology, Regenerative Medicine Research Center, Frontiers Science Center for Disease-related Molecular Network, West China Hospital of Sichuan University, Chengdu, China

^b Department of Nephrology, West China Hospital of Sichuan University, Chengdu, China

^c Department of Integrated Traditional Chinese and Western Medicine, West China Hospital of Sichuan University, Chengdu, China

ARTICLE INFO

Keywords:

Macrophage
Extracellular vesicle
Cytokine storm
Infection
SARS-CoV-2

ABSTRACT

Cytokine storms are a primary cause of multiple organ damage and death after severe infections, such as SARS-CoV-2. However, current single cytokine-targeted strategies display limited therapeutic efficacy. Here, we report that peritoneal M2 macrophage-derived extracellular vesicles (M2-EVs) are multitarget nanotherapeutics that can be used to resolve cytokine storms. In detail, primary peritoneal M2 macrophages exhibited superior anti-inflammatory potential than immobilized cell lines. Systemically administered M2-EVs entered major organs and were taken up by phagocytes (e.g., macrophages). M2-EV treatment effectively reduced excessive cytokine (e.g., TNF- α and IL-6) release *in vitro* and *in vivo*, thereby attenuating oxidative stress and multiple organ (lung, liver, spleen and kidney) damage in endotoxin-induced cytokine storms. Moreover, M2-EVs simultaneously inhibited multiple key proinflammatory pathways (e.g., NF- κ B, JAK-STAT and p38 MAPK) by regulating complex miRNA-gene and gene-gene networks, and this effect was collectively mediated by many functional cargos (miRNAs and proteins) in EVs. In addition to the direct anti-inflammatory role, human peritoneal M2-EVs expressed angiotensin-converting enzyme 2 (ACE2), a receptor of SARS-CoV-2 spike protein, and thus could serve as nanodecoys to prevent SARS-CoV-2 pseudovirus infection *in vitro*. As cell-derived nanomaterials, the therapeutic index of M2-EVs can be further improved by genetic/chemical modification or loading with specific drugs. This study highlights that peritoneal M2-EVs are promising multifunctional nanotherapeutics to attenuate infectious disease-related cytokine storms.

1. Introduction

Infectious diseases, caused by various types of pathogens (e.g., bacteria, viruses, fungi and parasites), have been a huge public health problem worldwide and can affect ~10% of all patients per year according to the World Health Organization report [1]. Although mild infections may be eliminated by the host immune system, severe infections frequently trigger immune disorders and a hyperinflammatory status, which is also known as cytokine storm [2,3]. Cytokine storms, characterized by excessive release of proinflammatory cytokines (e.g.,

IL-6 and TNF- α) and chemokines (e.g., MCP-1 and CCL5), have been recognized as one of the leading causes for the development of multiple organ damage and failure after severe infections [4,5]. For example, the recent COVID-19 pandemic caused by severe acute respiratory syndrome coronavirus 2 (SARS-CoV-2) is highly accompanied by elevated levels of cytokines (e.g., TNF- α and IL-6, ~2–5 fold vs. normal healthy), which are mainly secreted by disordered immune cells (e.g., macrophages) in patients, and this effect is primarily responsible for the subsequent acute respiratory distress syndrome and high mortality (up to ~9.6%) [6]. Therefore, therapeutics that can effectively resolve

* Corresponding author at: NHC Key Laboratory of Transplant Engineering and Immunology, West China Hospital, Sichuan University, No. 1 Keyuan 4th Road, Gaopeng Ave, Chengdu 610041, China.

E-mail address: liujingping@scu.edu.cn (J. Liu).

<https://doi.org/10.1016/j.jconrel.2022.06.063>

Received 9 March 2022; Received in revised form 27 June 2022; Accepted 29 June 2022

Available online 6 July 2022

0168-3659/© 2022 Elsevier B.V. All rights reserved.

cytokine storms are urgently required in the clinic. Some therapies aimed at countering or neutralizing a single cytokine (e.g., IL-6 or TNF- α blockers) have been developed and have shown certain beneficial effects in preclinical models [7,8], but they have shown controversial results in clinical trials of COVID-19 treatment [9]. The possible reason is that single cytokine-targeted therapy may function well when this cytokine is the driving factor in this disease, while the mechanisms of cytokine storms are complicated, and many cytokines are involved [3]. Instead, novel therapies that target multiple proinflammatory pathways might be more efficient, since the basic consensus is that cytokine storms are a result of disrupted networks involving multiple immune cells and cytokines.

Macrophages are the primary innate immune cells participating in host defense after pathogen infections and are distributed widely *in vivo* to sustain tissue homeostasis. In fact, the abnormal activation of macrophages has been linked to cytokine storms caused by severe infections and autoimmune diseases, which is also known as macrophage activation syndrome [10,11]. Macrophages are heterogeneous immune cells and can be roughly divided into two subtypes: M1-like macrophages (M1-M ϕ) and M2-like macrophages (M2-M ϕ). M1-M ϕ are mainly involved in proinflammatory processes, and hyperactivated M1-M ϕ are the major source of numerous cytokines (such as IL-6 and TNF- α) to trigger tissue damage after infections [10]. In contrast, M2-M ϕ mainly play anti-inflammatory and tissue repair roles. For example, we and others have found that M2-M ϕ transplantation could reduce proinflammatory cytokine (e.g., IL-6 and TNF- α) production in mouse models of acute kidney injury and colitis [12]. However, as living cells, the transplantation of whole M2-M ϕ *in vivo* is largely limited by several potential problems. For example, the viability and/or bioactivity of M2-M ϕ may change by storage and shipment conditions, and the phenotype of transplanted M2-M ϕ may return to M1 due to oxidative stress and inflammatory microenvironments *in vivo*. Thus, more stable, convenient and safe therapies are needed.

Extracellular vesicles (EVs) are a group of nanovesicles (~30–1000 nm) secreted by living cells. EVs possess bioactive properties similar to those of donor cells due to the various types of biomolecules (proteins, nucleic acids, lipids, metabolites, etc.) they are carried during biogenesis [10,13]. For example, EVs from bone marrow-derived M2 macrophages reduced proinflammatory cytokine (e.g., IL-1 β and IL-6) production in models of colitis and sepsis [14,15]. As a type of natural nanovesicle released by cells, EVs exhibit several advantages, such as lower

immunogenicity/toxicity and higher tissue penetrability than whole cells and synthetic nanoparticles [13]. Moreover, EVs remain bioactive after long-term storage, repeated freeze/thaw cycles and other harsh handling conditions [13]. However, several questions need to be addressed before further translation of M2-EV based therapies into clinical applications, especially in preventing infection-related cytokine storms. For example, the selection of proper EV resources (cell lines or primary cells), the therapeutic capacity of EVs in infectious models, and the remaining unclear comprehensive mechanisms of EVs.

Here, we report that primary peritoneal M2-EVs are efficient in reducing cytokine storms and their related oxidative stress and multiple organ damage in mice challenged with bacterial endotoxin. M2-EVs carry many functional miRNAs/proteins and thus simultaneously inhibit multiple essential proinflammatory pathways by regulating complex miRNA-gene and gene-gene networks. In addition, human peritoneal M2-EVs expressed angiotensin converting enzyme 2 (ACE2) and could serve as nanodecoys to prevent SARS-CoV-2 viral infection *in vitro*, while this effect was absent in MSC-EVs and dexamethasone (Dex) (a corticosteroid anti-inflammatory drug used in the clinic). Altogether, our results suggest that M2-EVs are promising multitarget nanotherapeutics to attenuate cytokine storms caused by severe infections, such as COVID-19 (See Fig. 1.).

2. Materials and methods

2.1. Cell culture

Primary mouse peritoneal macrophages (mM ϕ) were isolated from the peritoneal dialysis (PD) model of 8-week-old male C57BL/6 mice as previously described [16]. The isolated macrophages were cultured in RPMI 1640 medium (Gibco, CA, USA) supplemented with 10% heat-inactivated fetal bovine serum (FBS, Gibco), penicillin (50 U/mL), streptomycin (50 μ g/mL) and recombinant mouse macrophage colony-stimulating factor (mM-CSF, 20 ng/mL, Novoprotein). Primary mM ϕ and mouse macrophage cell lines (RAW264.7) were induced to M2 by incubating with recombinant mouse IL-4 and IL-13 (mIL-4/mIL-13, 20 ng/mL each, Novoprotein) proteins for 48 h. Human peritoneal macrophages (hPM ϕ) were isolated from dialysate of PD patients as previously described [17] and cultured in RPMI 1640 medium (Gibco) with 10% FBS (Gibco), penicillin (50 U/mL), streptomycin (50 μ g/mL) and recombinant human M-CSF (hM-CSF, 20 ng/mL, Novoprotein). hPM ϕ

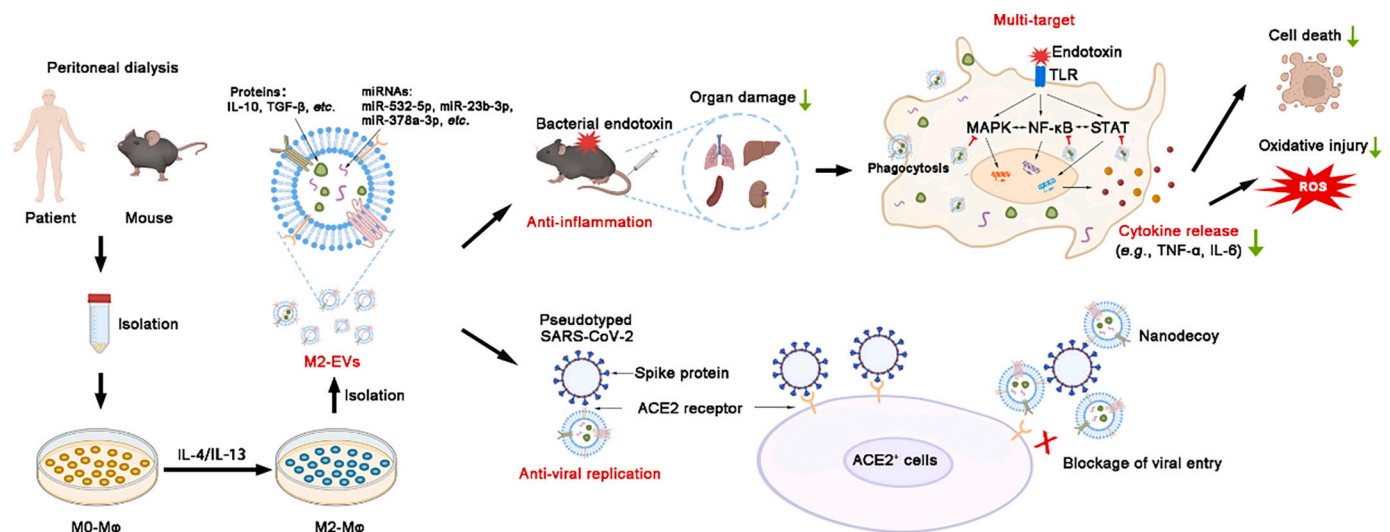


Fig. 1. Schematic diagram of the findings of this study. Large amounts of macrophages can be isolated from peritoneal dialysates of patients and mice. M2-EVs from peritoneal M2 macrophages carry many functional cargos and thus efficiently attenuate endotoxin-induced cytokine storms and organ damage by inhibiting multiple essential proinflammatory pathways. Moreover, human M2-EVs can also serve as nanodecoys to block viral entrance and replication in cells due to the expression of ACE2 (a receptor of SARS-CoV-2 spike protein).

were induced to M2 by incubating with recombinant human IL-4 and IL-13 (hIL-4/hIL-13, 20 ng/mL each, Novoprotein) proteins for 48 h. Patient dialysate sample collection and human cell experiments were conducted according to the National Institutes of Health (NIH) guidelines and approved by the Ethics Committee Biomedical Research, West China Hospital of Sichuan University (Permit NO. 20201019).

Mouse MSCs (mMSCs) were isolated from the bone marrow of 2-week-old male C57BL/6 mice as described previously [18], and human MSCs (hMSCs) were obtained from Sichuan Neo-life Stem Cell Biotech & Sichuan Stem Cell Bank (Chengdu, China). MSCs were cultured in Dulbecco's modified Eagle medium (DMEM, Gibco) in a humidified atmosphere at 37 °C with 5% CO₂ supplemented with 10% FBS (Gibco), penicillin (50 U/mL) and streptomycin (50 µg/mL), and cells at passages 3–4 were used for EV isolation.

2.2. EV isolation and characterization

EV-depleted medium was prepared by ultracentrifugation (120,000 ×g, 16 h, 4 °C) as described previously [18]. For collection of conditioned medium, M2 or MSCs were washed with PBS and cultured in EV-depleted medium for 48 h. EVs were isolated from the culture medium of cells using a differential ultracentrifugation method. Briefly, the medium was centrifuged at 300 ×g for 15 min and 2000 ×g for 15 min at 4 °C, followed by ultracentrifugation at 110,000 ×g for 90 min at 4 °C on an Optima XPN-100 ultracentrifuge with an SW32Ti rotor (Beckman Coulter, Brea, CA, USA). The isolated EVs were washed with PBS and subjected to a secondary ultracentrifugation (110,000 ×g for 90 min at 4 °C). The pure EV pellets were resuspended in PBS and stored at –80 °C until further use.

The morphology of EVs was observed by transmission electron microscopy (TEM, H-600, Hitachi, Ltd., Tokyo, Japan) as previously described [18]. The size distribution of EVs was analyzed using a Nanoparticle Tracking Analyzer (NTA, Particle Metrix, Meerbusch, Germany) as described previously [18]. The EV protein was quantified using a BCA protein assay kit (CWBIO, Beijing, China). EV purity was calculated by the ratio of EV particles to cell protein mass as previously reported [19]. Western blotting was performed to detect positive markers (anti-TSG101, anti-Alix, anti-HSP70) and negative markers (GM130) of EVs.

2.3. Cellular uptake assay of EVs

M2-Mφ or mMSC-derived EVs were labeled with PKH26 (Sigma Aldrich, St. Louis, MO, USA) according to the manufacturer's protocols. mMφ cells were incubated with PKH26-labeled EVs (10 µg/mL) for 4 h at 37 °C with 5% CO₂. After incubation, the cells were washed twice with PBS and stained with phalloidin (Yeasen Biotechnology, Shanghai, China) according to the manufacturers' instructions. The stained cells were observed using a confocal laser scanning microscope (N-STORM & A1, Nikon, Tokyo, Japan). To determine the cellular uptake mechanism of M2-EVs, cells were pretreated with inhibitors including Bafilomycin A1 (10 nM, Glpbio Technology, Montclair, CA, USA), Cytochalasin D (0.5 µM, Glpbio Technology), and Wortmannin (0.5 µM, Glpbio Technology) for 30 min, and then incubated with PKH26-labeled EVs. After incubation for 4 h, the cells were stained with phalloidin and observed using a confocal laser scanning microscope (Nikon).

2.4. In vitro cytokine release model and EV treatments

Primary mMφ were treated with LPS (40 ng/mL, Novoprotein) and IFN-γ (20 ng/mL, Novoprotein) for 4 h at 37 °C with 5% CO₂ to induce cytokine release. For EV functional evaluation, M2-EVs or MSC-EVs (10, 20 µg/mL) were added at the same time as LPS/γ-IFN treatment. After incubation, the treated cells were collected for qPCR assay. To determine whether the results were reproducible, LPS/γ-IFN-primed macrophages were treated with different EV preparations of M2-PMφ or MSCs,

and the expression of cytokines was analyzed.

2.5. In vivo biodistribution of EVs in mice

M2-Mφ or MSC-EVs were labeled with sulfo-Cy7-NHS ester according to the manufacturer's instructions (New Research Biosciences Co., Ltd., Xi'an, China). The unbound dyes were removed using an Exosome Spin Column (MW3000, Invirogen). Cy7-labeled M2-EVs or MSC-EVs (Cy7-EVs, 80 µg in 100 µL PBS per mouse) and an equal amount of free Cy7 (dye alone, negative control) were intravenously injected (*i.v.*) into C57/BL6 mice *via* the tail vein. At the indicated time points after injection, the mice were sacrificed by an overdose of pentobarbital sodium anesthesia, and the organs, including the hearts, lungs, livers, kidneys, and spleens, were collected and observed using an IVIS Spectrum optical imaging system (Perkin Elmer, Waltham, MA, USA). The intensity of fluorescence was quantified by Analyze 12.0 software (Perkin Elmer). To detect the distribution of EVs in organs, frozen sections of lung, liver, and spleen were made and costained with anti-CD68 (Abcam, ab201340) and DAPI (Sigma). Digital images of the stained sections were captured using a confocal laser scanning microscope (Nikon).

2.6. In vivo model of cytokine storm and EV treatments

All animal experiments were conducted according to the National Institutes of Health (NIH) guidelines and approved by the Animal Care and Use Committee of West China Hospital, Sichuan University (Permit NO. 2021020A). Male C57BL/6 mice (~20–25 g) were purchased from the Experimental Animal Center of Sichuan University (Chengdu, China). Animals were housed in individual cages with controlled temperature, humidity, and 12 h cycles of light and dark, and fed standard chow and tap water *ad libitum*. Mice were randomly divided into four groups ($n = 6–9$): healthy control (CON), LPS, LPS + M2-EVs, and LPS + MSC-EVs. A mouse model of cytokine storm was induced by intraperitoneal (*i.p.*) injection with LPS (5 or 10 mg/kg, in 100 µL PBS, Sigma). For EV treatments, mice pretreated with LPS were intravenously injected with M2-EVs or MSC-EVs (80 µg in 100 µL PBS per mouse) at 15 min after modeling. For detection of cytokine levels, serum and tissues were collected from mice at 4 h after EV treatment. For analysis of immune cell populations, spleens were collected at 4 h after EV treatment. To evaluate the degree of organ damage, tissues including lung, liver, spleen and kidney were collected at 24 h after EV treatment.

2.7. ELISA analysis of cytokine levels

The cytokine (TNF-α and IL-6) levels in cell culture medium or serum samples were analyzed using commercial ELISA kits for mouse TNF-α (Dakewe, Beijing, China) and mouse IL-6 (Dakewe) according to the manufacturer's instructions. In brief, 50 µL of sample or standard was added to each well of a 96-well plate, and then incubated with anti-TNF-α or anti-IL-6 at 37 °C for 90 min. Each well was incubated with streptavidin-HRP at 37 °C for 30 min. After incubating with TMB and stop solution, the 96-well plate was measured at 450 nm using a microplate reader (BioTek Instruments, Ink, USA).

2.8. Western blot analysis

Cell samples or EV samples were lysed in radioimmunoprecipitation assay (RIPA) buffer supplemented with protease inhibitors (Calbiochem, CA, USA) and phosphatase inhibitors (Calbiochem). The total protein concentration was determined using a BCA Protein assay kit. Equal amounts of proteins were electrophoresed on 12% sodium dodecyl sulfate-polyacrylamide gels (SDS-PAGE) and then transferred to polyvinylidene difluoride membranes (PVDF, Millipore, USA). The PVDF membrane was blocked with 5% skim milk buffer and then incubated with one of the following primary antibodies: mouse anti-HSP70

(ab2787, Abcam, Cambridge, MA, USA), rabbit anti-TSG101 (14497–1-AP, Proteintech, Rosemont, IL, USA), rabbit anti-Alix (12422–1-AP, Proteintech), rabbit anti-GM130 (12480, Cell Signaling Technology, Beverly, MA, USA), rabbit anti-HGF (26881–1-AP, Proteintech), rabbit anti-IL-10 (20850–1-AP, Proteintech), rabbit anti-SOD2 (24127–1-AP, Proteintech), rabbit anti-TGF- β (21891–1-AP, Proteintech), mouse anti-ACE2 (66699–1-Ig, Proteintech), and rabbit anti-Flag (AE004, Abclonal Biotech Co., Ltd., Cambridge, MA, USA) overnight at 4 °C. The PVDF membranes were incubated with HRP-conjugated secondary antibodies at 37 °C for 1 h. The protein bands on the PVDF membranes were observed using an enhanced chemiluminescence kit (Millipore) and quantified using ImageJ software (NIH, Bethesda, MD, USA).

2.9. RNA extraction and real-time PCR assay

Total RNA was extracted using TRIzol reagent (Gibco, Life Technologies) and reverse-transcribed into cDNA using a HiScreiptQ RT SuperMix kit (Vazyme Biotech, Nanjing, China). Real-time polymerase chain reaction (PCR) was performed on a CFX96 real-time PCR detection system (Bio-Rad, Hercules, CA, USA) with SYBR Green PCR mix (Vazyme Biotech). The primers used in this study are listed in Table S1. The data were analyzed using Bio-Rad CFX Manager software, and the relative changes of in mRNA were calculated by the delta-delta Ct method with GAPDH as the internal reference gene.

2.10. Flow cytometric analysis (FCA)

The FCA samples of mouse spleen were prepared as previously reported [16]. In brief, mouse spleen tissues were ground in PBS and then passed through a 70 μ m filter. Spleen samples were then incubated in red blood cell lysis buffer (R1010, Solarbio, Beijing, China) for 20 min to lyse red blood cells, followed by resuspension of the spleen sample with PBS. The prepared single-cell suspension from spleen was stained with FVS (564997, BD Pharmigen, San Diego, CA, USA), APC-CyTM7 Rat anti-mouse CD45 (557659, BD), PE Rat anti-mouse F4/80 (565410, BD), APC anti-mouse CD11c (117310, Biolegend, San Diego, CA, USA), FITC Hamster anti-mouse CD3e (553061, BD), PerCP/Cyanine5.5 anti-mouse CD4 (100434, Biolegend) and PE-CyTM7 Rat anti-mouse CD8a (552887, BD) for 30 min. After washing with PBS, the stained cells were analyzed using a flow cytometer (BD Bioscience, San Diego, CA, USA).

2.11. Histological examination

Mouse tissues fixed in 4% paraformaldehyde were embedded in paraffin and sliced into 4 μ m thick sections for hematoxylin and eosin (H&E) staining and immunohistochemistry (IHC) staining. For IHC, tissue sections were deparaffinized in xylene and rehydrated in graded ethanol, and the antigens were retrieved with citrate buffer. After inactivation of endogenous peroxidase with 3% H₂O₂, sections were blocked with 1% bovine serum albumin (BSA), incubated with diluted rabbit anti-ICAM-1 (10831–1-AP, Proteintech) overnight at 4 °C, and then stained with horseradish peroxidase (HRP)-conjugated secondary antibodies (Abclonal) and 3,3-diaminobenzidine (DAB) substrate. Images of stained sections were captured with a light microscope (Zeiss, AX10 imager A2, Oberkochen, Germany) and quantified using NIH ImageJ software.

2.12. TUNEL staining of tissues

Terminal deoxynucleotidyl transferase dUTP nick end labeling (TUNEL) staining was carried out with a commercial kit (Promega, Madison, WI, USA) following the manufacturer's instructions, and nuclei were stained with DAPI (Sigma, USA). The stained lung, liver and spleen sections were observed under a fluorescence microscope. The average number of TUNEL⁺ cells in 10 fields of each section was quantified with fluorescence intensity using NIH ImageJ software.

2.13. Immunofluorescent staining

After fixation (4% paraformaldehyde for 10 min), permeabilization (0.3% Triton X-100 for 10 min), and blocking (1% BSA for 1 h), cells or sections were incubated with mouse anti-8-OHdG (sc-393871, Santa Cruz Biotechnology, Dallas, TX, USA), anti-mouse KIM-1 (AF1817, R&D Systems, Minneapolis, MN, USA), anti-mouse CD68 (ab201340, Abcam) and anti-human ACE2 (266699–1-Ig, Proteintech) overnight at 4 °C. After washing with PBS, slides were incubated with fluorescein isothiocyanate (FITC)-conjugated secondary antibody (A11017, Life Technologies, CA, USA) at 37 °C for 1 h. Nuclei were visualized by staining with DAPI. Digital images were captured using a confocal laser scanning microscope (Nikon).

2.14. mRNA sequencing analysis of cells

Total RNA of the cells was extracted using TRIzol and then treated with DNase I (Takara, Shiga, Japan) to deplete the genomic DNA according to the manufacturer's instructions. High-quality RNA determination by 2100 Bioanalyzer (Agilent, USA) and quantification by ND-2000 (NanoDrop Technologies, USA) were used to construct a sequencing library. The RNA sequencing transcriptome library was prepared following the TruSeqTM RNA Sample Preparation Kit from Illumina (San Diego, CA). cDNA was synthesized using a SuperScript double-stranded cDNA synthesis kit (Invitrogen) with random hexamer primers (Illumina). Libraries were size selected for cDNA target fragments of 300 bp on 2% Low Range Ultra Agarose followed by PCR amplification using Phusion DNA polymerase (New England Biolabs, Ipswich, MA, USA). The expression of each transcript was calculated according to the transcripts per million reads method. The PCA, volcano plot, and heatmap were generated using an online platform (<https://www.omicsolution.org/wkomics/main/>).

2.15. miRNA sequencing analysis of M2-EVs

Total RNA of M2-EVs was extracted using TRIzol and then treated with DNase I to deplete the genomic DNA. The Multiplex Small RNA Library Prep Set (New England Biolabs) was used to produce small RNA libraries. cDNAs were prepared using adaptor-specific primers, and DNA fragments (~140–160 bp) were recovered. The library quality was evaluated using DNA High Sensitivity Chips on an Agilent Bioanalyzer 2100 system. Sequencing of libraries was conducted on an Illumina Novaseq 6000 system and 50 bp single-end reads were generated. All identical sequences with sizes of 18 to 32 nt were counted and removed from the initial data set. After elimination of nonmiRNAs (rRNA, tRNA, snoRNA, etc.), the expression of miRNAs was analyzed using the perfectly matched sequences from the BLAST search of miRbase (version 21.0). The cluster plot of miRNAs was generated by an online platform (<https://www.omicsolution.org/wkomics/main/>). The miRNA-gene interaction was analyzed using miRNet (<https://www.mirnet.ca/>) [20].

2.16. miRNA inhibition assay

To determine the role of each miRNA in regulating cytokine production, PM ϕ was first transfected with individual miRNA inhibitors (10 nM, miR-21a-5p, miR-23b-5p, miR-342-5p, miR-378a-3p, miR-532-5p, miR-6238 or let-7b-5p) using Lipo6000 (C0526, Beyotime, Shanghai, China) for 4 h as previously reported [21]. After that, these cells were challenged with LPS/ γ -IFN with or without M2-EV (10 μ g/mL) treatment. At the indicated times after incubation, the changes in cytokines (TNF- α and IL-6) and proinflammatory pathways (NF- κ B, JAK-STAT and p38 MAPK) in cells were analyzed.

2.17. In vitro SARS-CoV-2 pseudovirus infection assay

Human embryonic kidney cells (HEK-293 T cells) were transfected

with human ACE2 lentivirus (MOI = 40, Obio Technology, Shanghai, China) in the presence of polybrene (5 µg/mL, Obio Technology), and the expression of ACE2 in HEK293 cells was detected by western blotting and IF staining. The direct binding of SARS-CoV-2 pseudovirus (Obio Technology) to M2-EVs or MSC-EVs was observed using TEM as previously described [22]. For the SARS-CoV-2 pseudovirus infection assay, ACE2-overexpressing HEK-293 T cells (2×10^4 cells per well) were seeded in 48-well plates. SARS-CoV-2-GFP pseudovirus with lentiviral vector (MOI = 40) were spinoculated with hM2-EVs (10 µg/mL), hMSC-EVs (10 µg/mL) or dexamethasone (Dex, 0.5 µM) at 1200 ×g for 1.5 h at room temperature as previously reported [23], and the solution was then added to ACE2⁺ HEK-293 T cells. At 48 h after infection, the cells were washed, trypsinized and analyzed for GFP expression using a flow cytometer (BD Bioscience).

2.18. Statistical analysis

All data are presented as the mean ± SD and were analyzed with the *t*-test using GraphPad Prism 8.0.2 software (GraphPad Software Inc., San Diego, CA, USA); *p* < 0.05 was considered statistically significant.

3. Results and discussion

3.1. Primary M2 cells had stronger anti-inflammatory potency than immobilized cell lines

Macrophages are highly heterogeneous immune cells and are widely distributed in different tissues *in vivo*, and their bioactivities may vary in different cell sources. For example, peritoneal macrophages infiltrated faster to the liver injury sites than bone marrow-derived macrophages, which then contributed to local inflammation resolution [24]. According to previous studies, both primary macrophages (e.g., bone marrow-derived) and immobilized cell lines (e.g., mouse RAW264.7 cells) have been reported to produce M2-EVs. However, limited by the invasive surgery process and potential side effects, it is impossible to collect enough monocytes from the patients' bone marrow by biopsy in clinical practice. Instead, large amounts of leucocytes can be readily collected from dialysate, and monocytes/macrophages are the largest cell populations in human (~44% in leucocytes) or mouse (~47% in leucocytes) dialysate, which can be further induced to functional M1- or M2- macrophages *in vitro* [17]. Considering the superior yield and biofunctions, primary peritoneal M ϕ (PM ϕ) were selected in this study. Although the anti-inflammatory effects of primary M2 and cell line (e.g., RAW 264.7)-derived M2 have been reported [16,25], whether they have comparable efficiency remains unclear. Therefore, we first isolated and polarized mouse peritoneal M2 cells and compared their anti-inflammatory capacity with RAW-M2 cells. As shown in Fig. S1A–B, the purity of isolated mouse PM ϕ was up to 95.7%. After induction with IL-4/IL-13, mouse PM ϕ and RAW264.7 cells could be polarized toward the M2 subtype, as indicated by elevated gene expression of Arg1, Mrc1 and CCL17 (Fig. S1C–D).

It is well-documented that the anti-inflammatory effects of M2 cells are largely mediated by paracrine mechanisms, such as the release of cytokines and EVs [10,16]. Thus, the conditioned medium (containing cytokines and EVs) of cells was collected and used to evaluate their biofunction. As a key component of the gram-negative bacterial outer membrane, lipopolysaccharides (LPS) are commonly used to mimic bacteria-induced cytokine release *in vitro* [26]. LPS can be recognized by Toll-like receptors (TLRs) expressed on phagocytes (e.g., macrophages) and lead to the activation of downstream key proinflammatory pathways (e.g., MAPK and NF- κ B) and the subsequent release of excessive cytokines [16]. In LPS/IFN- γ -primed macrophages, conditioned medium from M2-PM ϕ or M2-RAW cells decreased cytokine (TNF- α and IL-6) expression in a dose-dependent manner (Fig. S2A). However, the M2-PM ϕ group showed a stronger inhibitory effect (~2-fold, vs. the M2-RAW264.7 group) on cytokine expression in LPS/IFN- γ -primed

macrophages (Fig. S2A). Macrophages exert their immunoregulatory effects mainly by paracrine mechanisms. For example, the released TGF- β has been shown to contribute to the anti-inflammatory role of M2-M ϕ [27]. In this study, M2-PM ϕ -secreted medium had a stronger inhibitory effect on cytokine expression, and M2-PM ϕ also showed higher potency to produce immunoregulatory factors (e.g., TGF- β) than M2-RAW264.7 cell line (Fig. S2B). Altogether, our results suggest that primary peritoneal M2 cells have stronger anti-inflammatory potency than immobilized cell lines and are more appropriate cell resources for M2-EV production.

3.2. M2-EVs effectively suppress endotoxin-induced cytokine release *in vitro*

Next, we isolated EVs from the culture medium of primary cells and analyzed their properties. The isolated M2-EVs and MSC-EVs had a typical bilayer lipid membrane structure (Fig. 2A), and their average sizes were ~ 150 nm and ~ 170 nm, respectively (Fig. 2B). These EVs were positive for marker proteins (Alix, TSG101 and HSP70) and negative for GM130 (a Golgi marker) expression (Fig. 2C). There was no significant difference in the purity between M2-EVs ($\sim 6.3 \times 10^{11}$ particles/mg) and MSC-EVs ($\sim 5.5 \times 10^{11}$ particles/mg) (Fig. S3A). EVs can regulate the function of target cells by delivering bioactive cargos, and thus the uptake of EVs by recipient cells is an essential step. Previous studies have found that the *i.v.* injected EVs were mainly taken up by phagocytes (e.g., macrophages) *in vivo* [28]. Therefore, we first assayed whether M2-EVs could enter PM ϕ and explored the possible uptake mechanism *in vitro*. M2-EVs were labeled with PKH26 (a lipophilic fluorescent dye), and then incubated with primary PM ϕ for 4 h. Then, positive signals of EVs (red) were observed in the cytoplasm of phalloidin-labeled cells (green), suggesting that M2-EVs were taken up by PM ϕ (Fig. 2E). The mechanisms of EV uptake by recipient cells are complicated and multiple pathways involved, such as macropinocytosis, endocytosis, and phagocytosis, have all been reported to play a part in EV uptake [29]. To explore the possible pathways that mediate M2-EVs uptake, PM ϕ were pretreated with potential inhibitors including bafilomycin A1 (Bal-A1), cytochalasin D (Cyto-D) and wortmannin (Wtmn) as previously reported [29] (Fig. 2D). It has been reported that Bal-A1 can block macropinocytosis by inhibiting endosomal and endosome-lysosomal fusion [29]; Cyto-D can block endocytosis by inhibiting actin polymerization [30]; and Wtmn can block phagocytosis by preventing pseudopod extension [31]. Compared to the vehicle (DMSO) group, the signals of M2-EVs (red) were decreased in the Bal-A1, Cyto-D and Wtmn treatment groups, and the lowest signal of M2-EVs was observed in the Wtmn treatment group (Fig. 2E–F). These results suggested that the uptake of M2-EVs in PM ϕ was regulated by multiple pathways, and that phagocytosis might be one of the main routes.

The inhibitory effects of the primary M2-EVs on cytokine release were further assayed *in vitro*, and another type of well-studied MSC-EV was chosen as the positive control, since MSC-EV therapies have been widely reported to reduce cytokine release in various inflammatory and infectious disease models [32,33]. Among many cytokines, the dramatic elevation of TNF- α and IL-6 has been most frequently reported in patients or animal models with cytokine storms. For instance, recent studies indicated that elevated IL-6 is highly associated with increased mortality in COVID-19 patients [9]. IL-6 is an activator of key proinflammatory pathways (e.g., JAK-STAT) and can induce the expression of many other cytokines (e.g., TNF- α and IL-8) as well as the differentiation of multiple immune cells (e.g., B cells and T cells) [34]. TNF- α is a vital acute phase protein induced by infections that can activate the proinflammatory NF- κ B pathway and act as an amplifier in the inflammatory cascade [3]. Increased TNF- α is positively correlated with mortality in disease conditions, such as lethal toxic shock [35]. In this study, we found that LPS/IFN- γ priming induced a dramatic increase in TNF- α (~60-fold) and IL-6 (~1000-fold) gene expression in macrophages compared to the control group (Fig. 2G). Conversely, M2-EV treatment

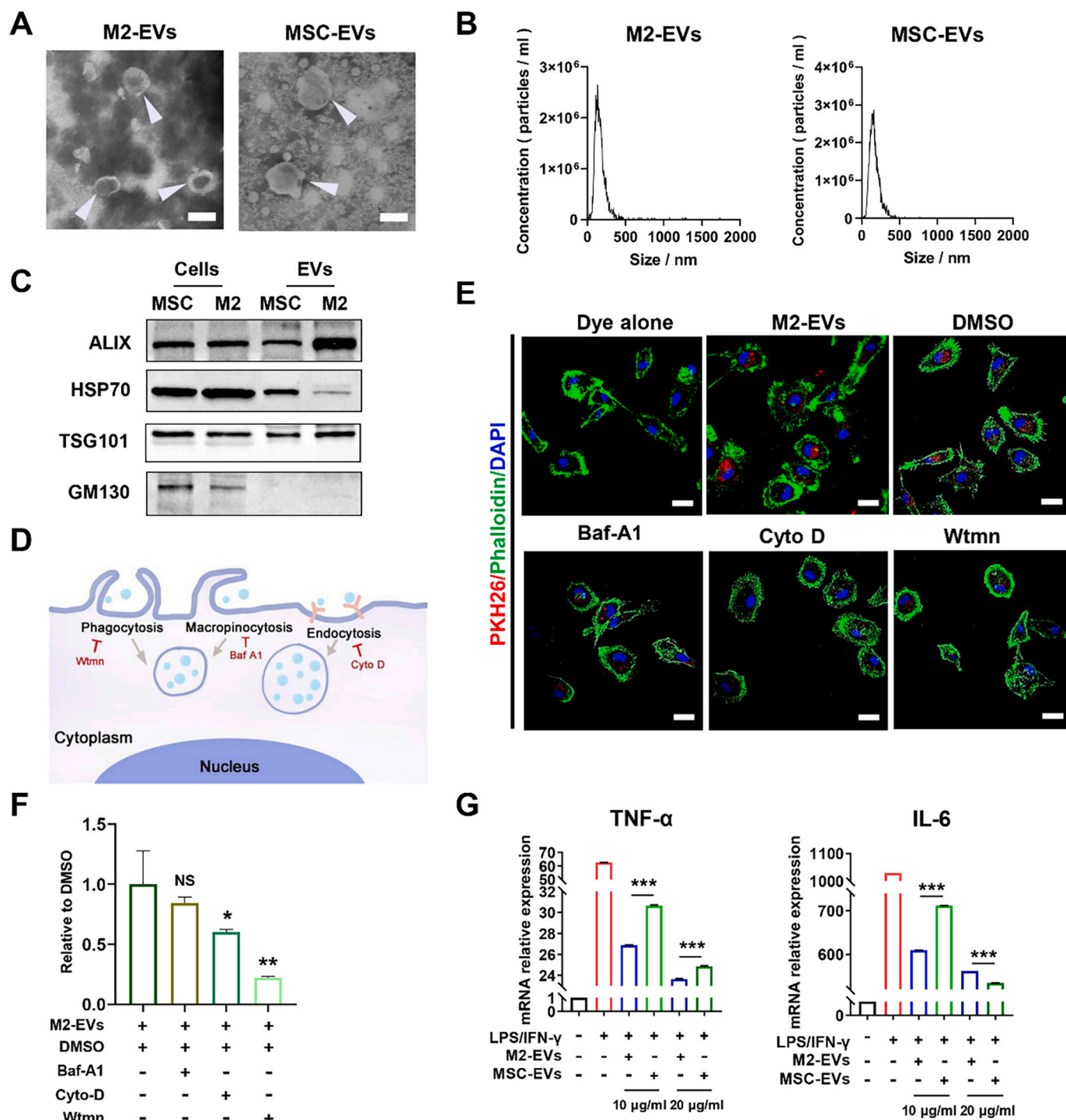


Fig. 2. Isolation and evaluation of the properties of M2-EVs *in vitro*. (A) Representative TEM images of EVs. The white arrow indicates EVs (scale bar = 200 nm). (B) Size distributions of EVs measured by NTA. (C) Western blot analysis of EV positive markers (ALIX, HSP70, TSG101) and negative markers (GM130). (D) Schematic illustration of the mechanisms of EV uptake. (E) Representative images of M2-EV uptake in PMφ stained with FITC Phalloidin (green) and DAPI (blue) (scale bar = 20 µm). Cells were pretreated with DMSO, Baf-A1 (Bafilomycin A1), Cyto D (Cytochalasin D) or Wtmn (Wortmannin) for 15 min and incubated with PKH26-labeled M2-EVs (red) for 4 h. (F) Relative uptake ratio of M2-EVs in PMφ of different groups (n = 3; *p < 0.05, **p < 0.01 vs DMSO group). (G) Measurement of TNF-α and IL-6 mRNA levels in LPS/IFN-γ-primed PMφ with or without EV treatments for 4 h by qPCR (n = 3; ***p < 0.001, M2-EVs vs MSC-EVs). (For interpretation of the references to colour in this figure legend, the reader is referred to the web version of this article.)

markedly decreased the expression of TNF-α (decreased by ~70% vs. the LPS/IFN-γ group) and IL-6 (decreased by ~60% vs. the LPS/IFN-γ group) in a dose-dependent manner. The MSC-EV group also showed considerable reductions in TNF-α and IL-6 expressions, but their inhibitory efficacy was lower than M2-EVs group at the same concentrations (Fig. 2G). We also performed repeated assays using different EV

preparations, and the results showed that the anti-inflammatory effects of M2-EVs and MSC-EVs were highly reproducible (Fig. S3B–C). These results suggest that M2-EVs can suppress endotoxin-induced excessive cytokine release *in vitro*.

3.3. M2-EVs attenuated the cytokine storm and macrophage hyperactivation *in vivo*

EVs can affect the functions of distal cells or tissues that are far from where they are secreted or administered. To visualize the biodistribution of systemically infused EVs, EVs were labeled with cyanine7 (a near-infrared dye, Cy7-EVs) and then injected into mice *via* the tail vein. In line with previous reports, we found that M2-EVs (Fig. 3A, C) and MSC-EVs (Fig. 3B, D) displayed a similar distribution pattern, primarily accumulating in the liver, spleen, lung, kidney and heart after *i.v.* injection. It has been reported that *i.v.* injected EVs are mainly taken up by phagocytes (e.g., macrophages) *in vivo* [28]. Consistently, we observed

the colocalization of Cy7-labeled M2-EVs with CD68⁺ macrophages in tissue sections, such as lung, liver and spleen (Fig. 3E). However, no detectable signal was observed in the dye control (Cy7 alone) groups (Fig. 3A-E). These results suggest that large amounts of M2-EVs can arrive at major organs and are taken up by macrophages after systemic injection.

To validate the *in vitro* findings, we also evaluated the therapeutic effects of EVs in a mouse model of LPS-induced cytokine storm (Fig. 4A). As a type of bacterial-derived endotoxin, LPS is a robust bacterial inducer of cytokine release *in vivo*, and low-dose injection of LPS into healthy human volunteers causes pathophysiologic alterations that are similar to those reported in patients with cytokine storms [36]. To better

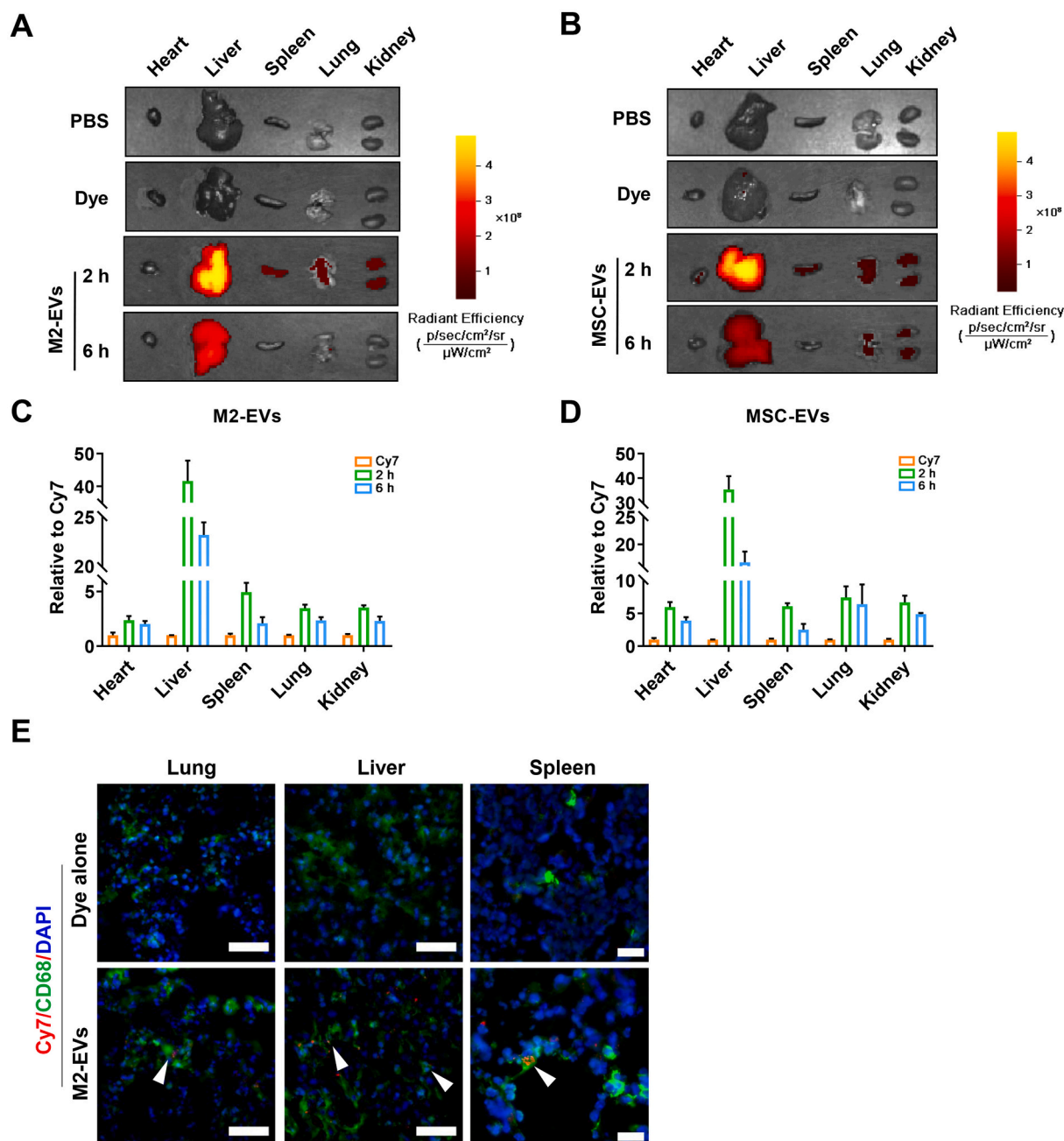


Fig. 3. *In vivo* biodistribution of EVs. (A–B) Representative IVIS images of organs harvested from mice at 2 and 6 h after intravenous injection of Cy7-labeled M2-EVs or MSC-EVs. Mice that received PBS and Cy7 dye alone were included as negative controls. (C–D) Quantification of the fluorescence intensity of M2-EVs or MSC-EVs in different organs of mice ($n = 3$). (E) Representative micrographs of Cy7-EVs (red) in tissue sections. Spleen tissues were costained with CD68⁺ macrophages (green) and DAPI (blue). The white arrow indicates the colocalization of green and red signals (scale bar = 50 μm for lung and liver, scale bar = 20 μm for spleen). (For interpretation of the references to colour in this figure legend, the reader is referred to the web version of this article.)

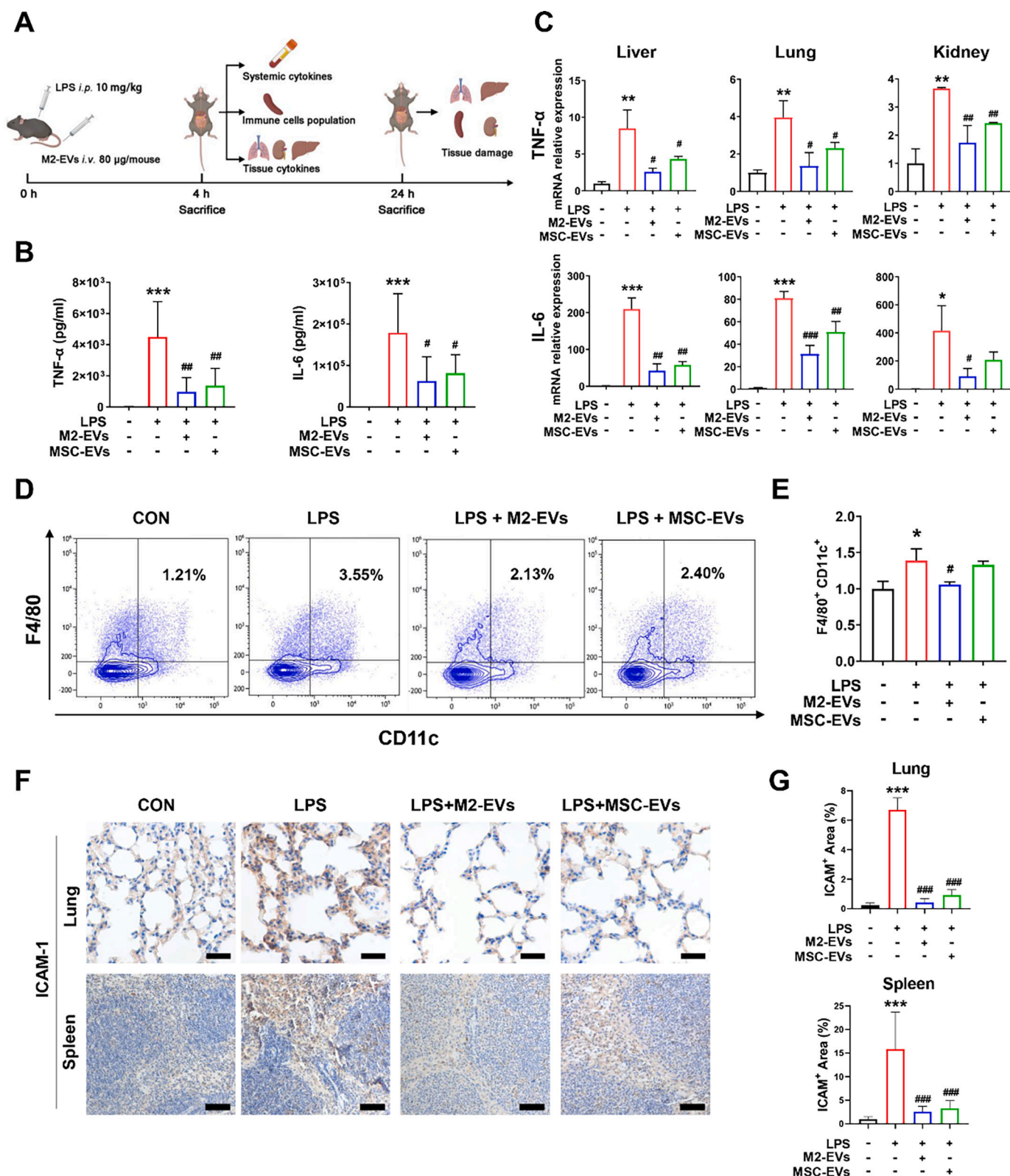


Fig. 4. Effects of M2-EVs on the inflammatory response *in vivo*. (A) Schematic illustration of animal experiments. (B) Measurement of mouse plasma TNF- α and IL-6 levels at 4 h after LPS challenge by ELISA ($n = 6-9$). (C) Quantification of mouse TNF- α and IL-6 mRNA levels in liver, lung and kidney tissues at 4 h after LPS challenge by qPCR ($n = 3$). (D) FCA analysis of immune cell population changes in spleen. (E) Quantification of the proinflammatory F4/80⁺/CD11c⁺ macrophage population in the spleen ($n = 3$). (F) Representative micrographs of ICAM-1 IHC staining of lung and spleen sections at 24 h after LPS challenge. (G) Quantification of tissue ICAM-1 protein expression detected by IHC staining ($n = 3$). (*** $p < 0.001$, ** $p < 0.01$, * $p < 0.05$ vs CON group; ### $p < 0.001$, ## $p < 0.01$, # $p < 0.05$ vs LPS group; scale bar = 20 μm for lung; Scale bar = 100 μm for spleen).

stimulate severe infections, we first detected the dynamic changes in the blood cytokine levels of mice in response to different doses of LPS (5 or 10 mg/kg) challenge. A higher dose of LPS (10 mg/kg) priming led to a rapid and dramatic elevation of plasma TNF- α and IL-6 levels compared to the control or lower dose (5 mg/kg) group (Fig. S4A–B). In line with the *in vitro* results, M2-EV treatment effectively reduced the systemic and local inflammatory degree *in vivo*, as indicated by the reduction in plasma cytokines (decreased by ~78% for TNF- α , decreased by ~65% for IL-6) and tissue cytokines (decreased by ~50–70% for TNF- α , decreased by ~60–80% for IL-6) levels in multiple organs (liver, lung and kidney) compared to the LPS groups (Fig. 4B–C). Moreover, the

expression of vital chemokines (e.g., ICAM-1) was suppressed by M2-EV treatment in lung, spleen and liver tissues (Fig. 4F, G). Similarly, we also observed a slightly higher anti-inflammatory efficacy in the M2-EV groups than in the MSC-EV groups at the same concentrations (Fig. 4B, C, F, G).

In infectious conditions, the overproduction of cytokines is mainly regulated by a complex network involving innate and adaptive immune cells, such as monocytes, macrophages, T cells and dendritic cells [3], and the populations of each cell type dynamically change in different stages or states after infections. To further explore the immunoregulatory role of M2-EVs, we detected changes in the immune cell populations

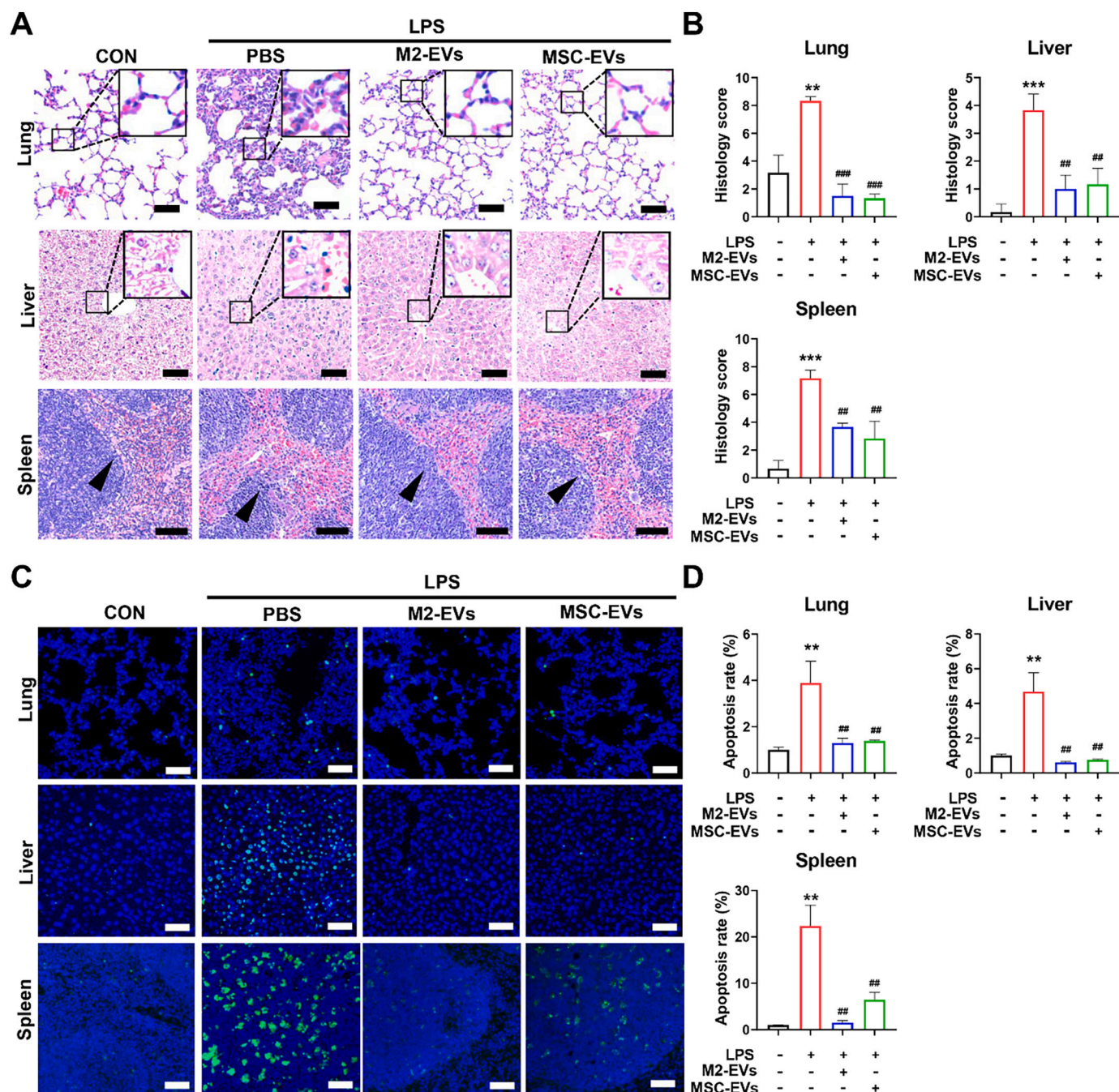


Fig. 5. Effects of M2-EVs on multiple organ damage *in vivo*. (A) Representative H&E staining micrographs of lung, liver and spleen sections at 24 h after LPS challenge (scale bar = 20 μ m for lungs and livers; scale bar = 100 μ m for spleens). The enlarged figures show the detailed changes in lung and liver sections and the black arrows in splenic micrographs show the loss in boundary definitions. (B) Quantification of histological injury scores of the lung, liver and spleen by professional pathologists ($n = 3$). (C) Representative TUNEL staining micrographs of the lung, liver and spleen sections at 24 h after LPS challenge (scale bar = 100 μ m). (D) Quantification of TUNEL⁺ cells in the lung, liver and spleen sections. ($n = 3$). (*** $p < 0.001$, ** $p < 0.01$ vs CON group; ### $p < 0.001$, ## $p < 0.01$ vs LPS group).

in organs (e.g., spleen) using a multiple staining flow cytometry analysis (FCA) method (Fig. S5). Indeed, the population of proinflammatory M1 macrophages (F4/80⁺/CD11c⁺) increased markedly in spleen at early stage (4 h) after LPS challenge, while its population was reduced by M2-EV treatment (Fig. 4D-E). MSC-EV treatment led to a slight reduction in proinflammatory macrophages (F4/80⁺/CD11c⁺) in the spleen (Fig. 4D, E). However, there was no significant difference between the

populations of CD45⁺ total leucocytes, CD3⁺ total T cells, CD4⁺ helper T cells and CD8⁺ cytotoxic T cells in the spleen tissues of mice at 4 h after LPS priming (Fig. S5B), suggesting that innate immune cells (e.g., macrophages) might be a major source of cytokines at the early phase after endotoxin challenge. These results suggest that M2-EVs can effectively reduce the endotoxin-induced cytokine storm *in vivo*, and this effect is at least partly induced by inhibiting hyperactivation of macrophages.

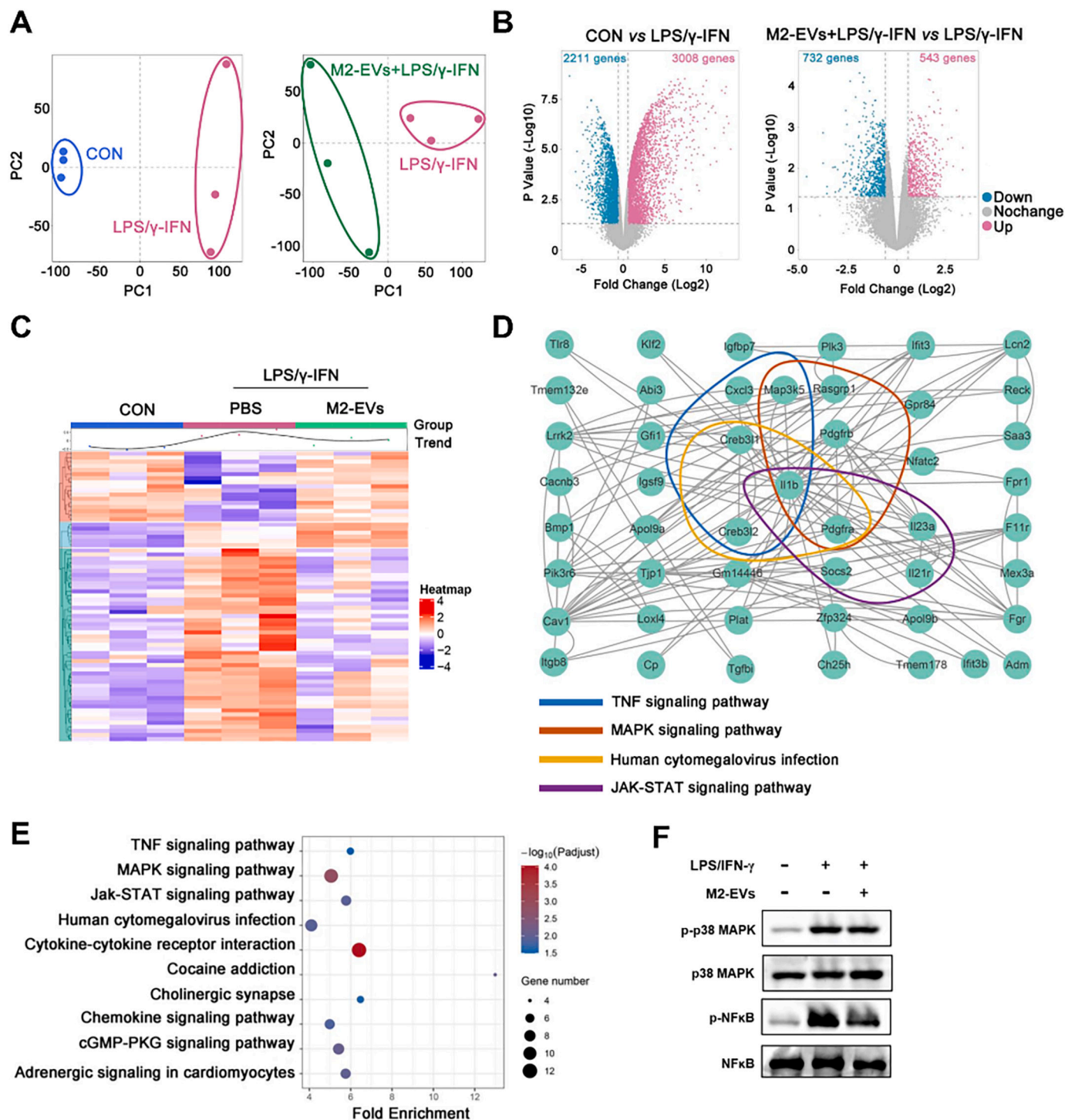


Fig. 6. Effects of M2-EVs on proinflammatory pathways *in vitro*. (A) PCA score plot representing discrepancies between groups (n = 3). (B) Volcano plot representing the significantly changed genes (fold change >2, p < 0.05). (C) Heatmap of the differentially expressed genes and the average expression curve above the heatmap. (D) Gene-gene interactions between the top 20 differentially expressed genes using STRING analysis. (E) KEGG pathway enrichment analysis based on the top 20 differentially expressed genes. (F) Western blot analysis of the total and phosphorylated levels of p38MAPK and NF-κB in LPS/IFN-γ-primed PMφ treated with M2-EVs for 1 h.

3.4. M2-EVs attenuated cytokine storm-associated multiple organ damage *in vivo*

Infection-induced cytokine storms are highly associated with multiple organ damage, such as acute lung, liver and kidney injury [37]. Thus, we also determined whether M2-EV treatment could protect multiple organs against inflammatory injury *in vivo*. After LPS challenge, we found clear pathological lesions, such as hemorrhage and inflammatory cell infiltrations in multiple organs (lung, liver and spleen) (Fig. 5A). Lung edema and thickened alveolar walls, liver necrosis, and dilated

spleen sinus with a disorganized white pulp with loss in boundary definitions and barely distinct follicular structure, were also observed in mice challenged with LPS (Fig. 5A). The levels of kidney injury molecule-1 (KIM-1, a marker of renal damage) were elevated in kidneys from the LPS group (Fig. S6A–B). In contrast, M2-EV treatment suppressed lesion formation in multiple organs, and reduced the overall tissue injury scores of the lung, liver and spleen in mice with LPS priming (Fig. 5B, S6B). Although M2-EVs have higher inhibitory potency on cytokine production *in vitro*, they showed a similar tissue protective effect to MSC-EVs *in vivo*, which may be because *in vivo* environments or

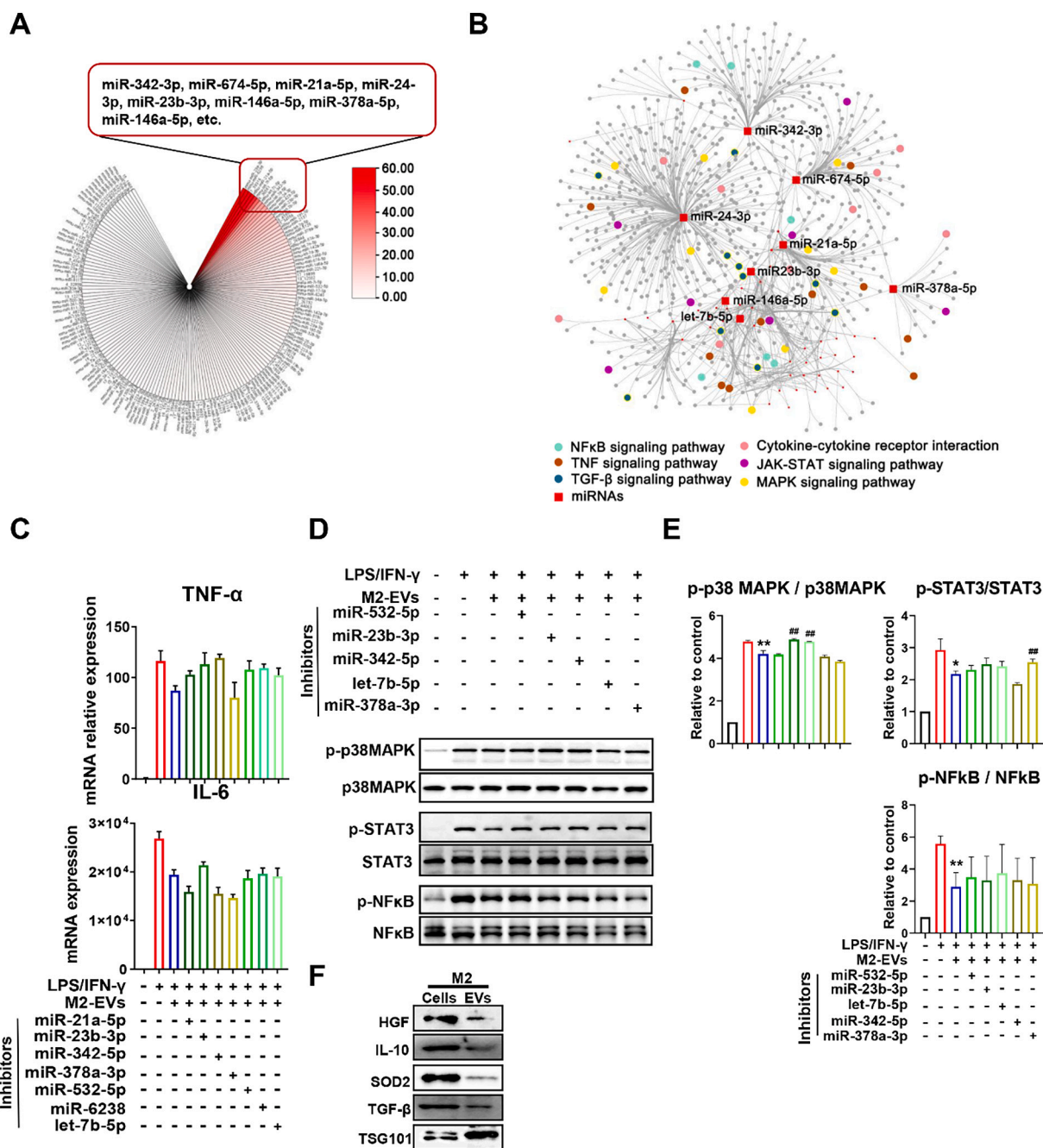


Fig. 7. M2-EVs inhibited cytokine production by mediating complex signaling networks. (A) An overview of miRNA contents within M2-EVs and the top 8 most abundant miRNAs are listed. (B) miRNA-gene network analysis and KEGG pathway enrichment analysis based on differentially expressed genes. (C) Measurement of cytokine TNF-α and IL-6 mRNA levels in LPS/IFN-γ-primed PMφ cotreated with M2-EVs and different miRNA inhibitors for 4 h. (D) Western blot analysis of the phosphorylation levels of p38MAPK, STAT3 and NF-κB in LPS/IFN-γ-primed PMφ cotreated with M2-EVs and miRNA inhibitors for 1 h. (E) Quantification of the phosphorylation levels of p38MAPK, STAT3 and NF-κB in different groups (n = 3; **p < 0.01, *p < 0.05 vs CON group; ##p < 0.01 vs LPS group). (F) Western blot analysis of HGF, IL-10, SOD2, TGFβ1 and TSG101 protein expression in M2 cells and EVs.

EV-tissue interactions in disease conditions are much more complicated than those in cell models. Nevertheless, our results demonstrate that peritoneal M2-EVs are potent therapeutics for inflammatory diseases.

Excessive cytokines can induce cell death by triggering oxygen reactive species (ROS) overproduction and proapoptotic signals, which in turn cause severe tissue damage and final organ failure [38]. Moreover, cytokines and oxidative stress often contribute to fueling each other via complicated feedbacks [18,39]. For example, TNF- α stimulation led to elevated mitochondrial ROS (mtROS) levels in lung epithelial cells [40]. In line with these reports, we found an increase in mtROS production in PM ϕ under LPS/ γ -IFN stimulation, and their levels were further reduced by M2-EV treatment (Fig. S7A). The levels of 8-hydroxydeoxyguanosine (8-OHdG, an oxidative injury marker) increased in the major organs (lung, liver and spleen) of mice at 24 h after LPS challenge and were neutralized by M2-EV treatment (Fig. S7B–C). Apoptotic cells in mouse tissues were also detected by terminal deoxynucleotidyl transferase dUTP nick end labeling (TUNEL) staining. Consequently, we observed elevated numbers of TUNEL⁺ apoptotic cells in the major organs (lung, liver and spleen) of mice that received LPS, whereas this elevation was markedly ameliorated by M2-EV treatment (Fig. 5C–D).

3.5. M2-EVs suppress cytokine production by inhibiting multiple proinflammatory pathways

To further reveal the underlying mechanisms, we analyzed the changes in the gene profiles of proinflammatory M ϕ receiving M2-EV treatment using RNA sequencing (RNA-seq). Principal component analysis (PCA) results showed an overall alteration in gene expression between groups (Fig. 6A). Compared with the control group, 3008 upregulated genes and 2211 downregulated genes were observed in the LPS/IFN- γ group. After M2-EV treatment, 543 upregulated genes and 732 downregulated genes were found compared to the LPS/IFN- γ group (Fig. 6B). Heatmap analysis showed that many upregulated genes induced by LPS/IFN- γ were neutralized by M2-EV treatment (Fig. 6C). Next, we performed gene-gene interaction analysis and KEGG pathway enrichment analysis to reveal the intracellular pathways affected by M2-EVs. Indeed, these differentially expressed genes between the LPS/IFN- γ group and the LPS/IFN- γ + M2-EVs group were mainly enriched in inflammation-associated pathways, such as cytokine-cytokine receptor interaction, JAK-STAT, MAPK, and NF- κ B pathways (Fig. 6D–E). Further western blotting results confirmed the activation of the NF- κ B, p38 MAPK and JAK-STAT pathways in LPS-treated macrophages, while these pathways were inhibited by M2-EV treatment (Fig. 6F, 7D). These results suggest that, instead of targeting a single cytokine, M2-EVs may suppress cytokine production by simultaneously inhibiting multiple essential proinflammatory pathways (e.g., NF- κ B, p38 MAPK and JAK-STAT).

Increasing evidence indicates that EVs can impact the functions of recipient cells by delivering multiple types of bioactive cargos, especially microRNAs (miRNAs) and proteins [10]. To explore the possible cargos responsible for the therapeutic roles of M2-EVs, we first detected the miRNA profile in M2-EVs by RNA-seq. A total of 601 miRNAs (including 445 known and 156 predicted miRNAs) were found in M2-EVs, and the top 8 miRNAs with the highest abundance were miR-342-3p, miR-674-5p, miR-24-3p, miR-21a-5p, miR-23b-3p, miR-146a-5p, miR-378a-5p and let-7b-5p (Fig. 7A). Next, we performed miRNA-gene network analysis to explore the possible interactions between these miRNAs carried by EVs and the intracellular genes regulated by M2-EVs (Fig. 7B). Again, the results indicated that these miRNAs might jointly regulate gene networks mainly enriched in proinflammatory pathways, such as cytokine-cytokine receptor interaction, JAK-STAT, MAPK, NF- κ B, TNF and TGF- β pathways (Fig. 7B). We further validated these findings using miRNAs inhibitors, which can specifically bind to endogenous miRNAs and thus inhibit their bioactivities. Indeed, the inhibitory effects of M2-EVs on cytokine (TNF- α and IL-6) production and proinflammatory pathways (NF- κ B, JAK-STAT3 and p38

MAPK) were abolished to some extent after pretreatment with individual miRNA inhibitors, such as miR-532-5p, miR-23b-3p, let-7b-5p, miR-342-5p and miR378a-3p (Fig. 7C–E). In fact, these miRNAs (e.g., miR-532-5p, miR-23b-3p and miR-378a-3p), have been shown to reduce cytokine release in inflammatory disease models [41,42]. The effect of miRNA inhibitor alone on cytokine expression in macrophages was also assessed, and most of them had no significant influence on IL-6 and TNF- α expression, while only let-7b-5p or miR-342-5p inhibitor increased individual cytokine levels to some extent (Fig. S8). Since macrophages also express miR-342-5p and let-7b-5p, which may have an anti-inflammatory role [43,44], the possible reason was that macrophages with endogenous miR-342-5p or let-7b-5p exhaustion were more susceptible to LPS/IFN- γ stimulation. Nevertheless, these results suggest that these miRNAs carried by M2-EVs can function in anti-inflammation, and they may exert therapeutic effects in a synergistic manner.

Furthermore, we detected the expression of some important protein cargos (e.g., IL-10, TGF- β , HGF and SOD2) in M2-EVs, since these proteins have been associated with the immunoregulatory or antioxidant effects of EVs [18,32]. Indeed, we found the presence of these proteins within M2-EVs (Fig. 7F), suggesting that these functional proteins might also partly contribute to the therapeutic effects of M2-EVs. Altogether, these results suggest that M2-EVs can inhibit multiple proinflammatory pathways by regulating complicated miRNA-gene and gene-gene networks, and this effect was likely a joint result of many functional miRNAs and proteins delivered by these EVs.

3.6. hM2-EVs served as nanodecoys to prevent SARS-CoV-2 pseudovirus infection *in vitro*

In addition to bacteria, other pathogens, such as many viruses, can also trigger cytokine storms. For example, in the recent COVID-19 pandemic, dramatic elevation of multiple cytokines, such as TNF- α , IL-6 and IFN- γ , was observed in the blood of patients with severe SARS-CoV-2 infection, and its severity was strongly associated with multiple organ injury and mortality [5,34]. Some immunosuppressive drugs, such as Dex, have shown certain effects on reducing cytokine levels in COVID-19 patients [45]. However, the overall immunosuppression and possible side effects (such as hypertension and osteonecrosis of the femoral head) caused by these drugs, may adversely reduce viral clearance and increase the risks of secondary infections [5,34]. Thus, novel therapies that can prevent SARS-CoV-2 replication and its associated cytokine production are urgently needed. The key step of SARS-CoV-2 entrance into cells is primarily mediated by the binding of the SARS-CoV-2 spike protein to the angiotensin-converting enzyme 2 (ACE2) receptor expressed on the cell surface [46]. Inspired by this process, therapeutic strategies that aim to block or neutralize the binding of SARS-CoV-2 to ACE2 have been proposed. For example, EVs derived from ACE2-overexpressing parent cells have been used as nanodecoys to protect against pseudotyped SARS-CoV-2 infections [23,47].

Interestingly, the expression of ACE2 receptor has been found on the surface of primary alveolar macrophages [48]. Based on these findings, we speculated that hM2-EVs may also express ACE2 and thus are capable of neutralizing SARS-CoV-2. Our results showed that large amounts (~25%) of human peritoneal macrophages (hPM ϕ) could be collected from the peritoneal dialysate of PD patients (Fig. S9A). These cells were further polarized toward the M2 phenotype *in vitro*, as indicated by elevated expression of Mrc1 and Arg1 (Fig. S9B–C). We isolated EVs from hPM ϕ and human MSCs, and the resulting hM2-EVs and hMSC-EVs were bilayer lipid membrane vesicles with average sizes of ~150 nm and ~170 nm, respectively (Fig. 8A–B). Both EVs expressed markers such as Alix and TSG101 (Fig. 8C). We found that hM2-PM ϕ and hM2-EVs highly expressed ACE2, while much weaker ACE2 expression was found in hMSCs and hMSC-EVs, which was consistent with a previous report that hMSCs had lower or negative ACE2 expression [49]. A recent study found direct binding of SARS-CoV-2 pseudovirus to ACE2-expressed biosynthetic cellular membrane vesicles using TEM [22].

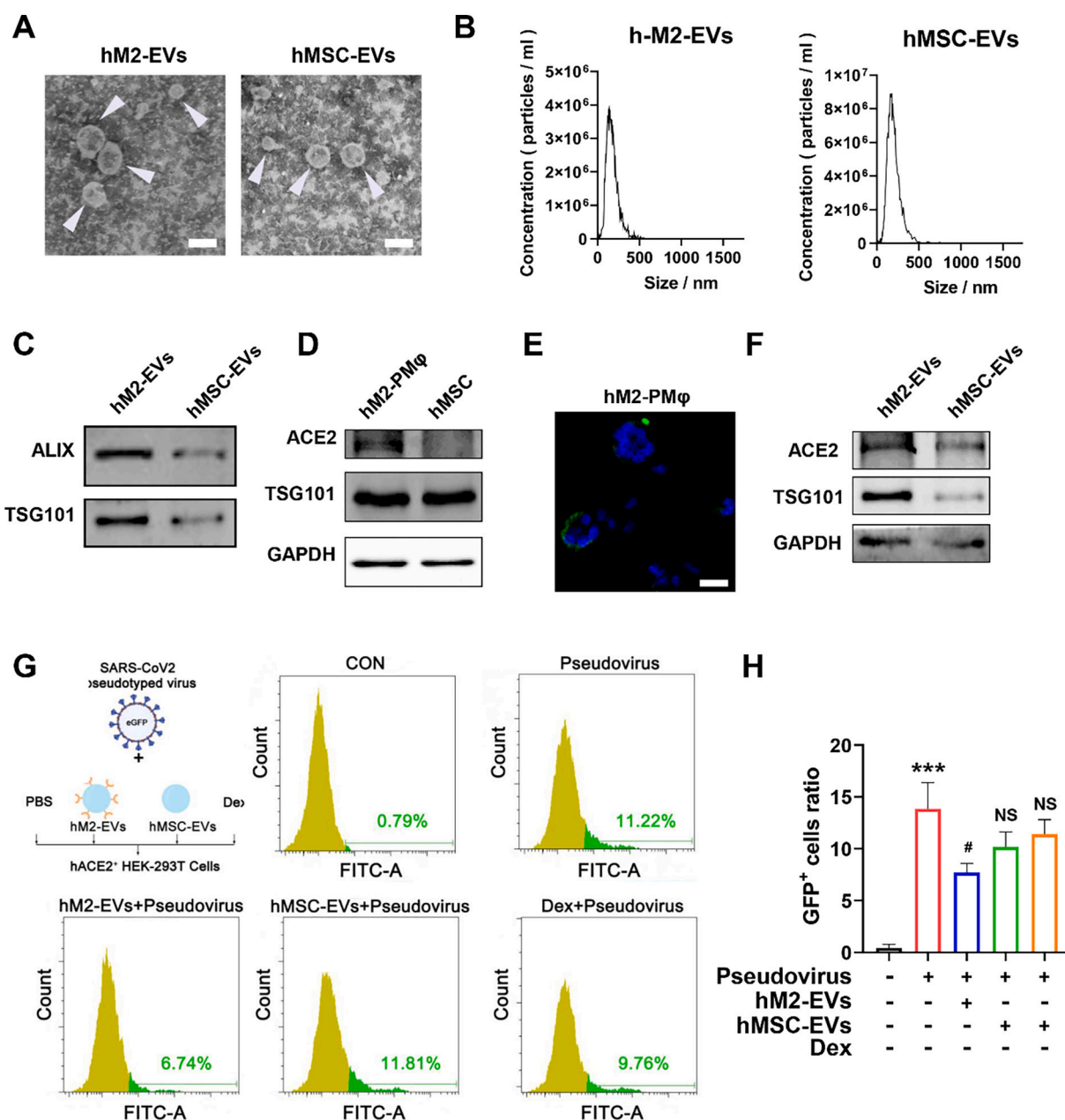


Fig. 8. Effects of M2-EVs on SARS-CoV-2 pseudovirus infection *in vitro*. (A) Representative TEM images of human EVs. The white arrow indicates EVs (scale bar = 200 nm). (B) Size distributions of human EVs measured by NTA. (C) Western blot analysis of positive marker proteins (ALIX and TSG101) in EV samples. (D) Western blot analysis of ACE2 protein expression in different cells. (E) Representative micrographs of ACE2 IF staining (scale bars = 20 μ m). (F) Western blot analysis of ACE2 protein expression in different EVs. (G) FCA analysis of the percentage of infected GFP⁺ ACE2-overexpressing 293 T cells after incubation with SARS-CoV-2 pseudovirus alone or in combination with hM2-EVs, hMSC-EVs or Dex for 48 h. (H) Quantification of the percentage of infected ACE2-overexpressing 293 T cells in different groups (n = 3; ***p < 0.001 vs CON group; #p < 0.05 vs Pseudovirus group; ^{NS}p > 0.05 vs Pseudovirus group).

Similarly, we also observed the binding of SARS-CoV-2 pseudovirus to hM2-EVs, while the effect was much weaker in hMSC-EVs (Fig. S10A). Next, we evaluated the potential of ACE2⁺ hM2-EVs in preventing SARS-CoV-2 pseudovirus infection *in vitro*. According to a previous report, ACE2-overexpressing 293 T cells were established and then incubated with SARS-CoV-2 pseudovirus containing a GFP reporter for the detection of infected cells (Fig. S10B-D). In addition to hM2-EVs, hMSC-EVs and Dex were also included in this experiment, since they have been proposed in clinical trials of SARS-CoV-2 patients [45,50]. As expected, elevated numbers of infected cells were observed in response to higher concentrations of SARS-CoV-2 pseudovirus (Fig. 8G-H). hM2-EV treatment significantly reduced the numbers of infected cells compared to pseudovirus treatment alone. However, neither hMSC-EVs nor Dex

treatment prevented pseudovirus infection in ACE2⁺ 293 T cells (Fig. 8G-H). Although the *in vivo* viral infection experiment cannot be performed due to the absence of an animal model and biosafety concerns, our results at least partly suggested that these ACE2⁺ hM2-EVs might serve as nanodecoys to neutralize SARS-CoV-2 and thus reduce the viral load in ACE2⁺ cells. In addition, we found that ACE2⁺ hM2-EVs could also reduce cytokine release in mPMφ challenged with LPS (Fig. S9D), which was similar to mouse M2-EVs. Taken together, our results indicate that peritoneal M2-EVs can not only directly suppress cytokine production by delivering multiple functional cargos, but can also serve as nanodecoys to prevent SARS-CoV-2 infection because of their surface ACE2.

Moreover, M2-EVs may have some additional advantages, such as

rich source, regulatory potential, and tropism effect, compared to commonly used MSC-EVs. To acquire large numbers of cells for EV production, *in vitro* long-term culture and expansion of MSCs are needed, which is costly and time-consuming (~1–2 months) and may also induce MSC senescence [51]. A large number of M2-PM ϕ (~10 million in 1 bag (~2 L) human dialysate) can be readily collected from multiple patients with peritoneal dialysis [17], which might become a rich source for EV production in the shorter term (~3–7 days in our study). Macrophages are regulatory immune cells that can be modulated into different functional subtypes (e.g., M2a, M2b, M2c), which admit them to produce more specific M2-EVs for different therapeutic purposes. EVs might have homing effects on their original cells or tissues. A recent study showed that M2-EVs exhibited a tropism effect on M2 cells in a mouse model of allergic asthma [52], suggesting that M ϕ -EVs may be favorable for macrophage-related immune diseases. As a type of cell-derived nanomaterial, the therapeutic potential of M2-EVs can be readily and precisely improved by genetic and chemical modifications, and loading with specific therapeutic reagents in response to different disease conditions. However, PM ϕ -EVs may also have some limitations. Peritoneal dialysis patients with end-stage kidney disease may have other complications or immune impairments, which might impair the viability or immune function of PM ϕ . Thus, the quality of dialysate (e.g., no infection or inflammation) and immunoregulatory effects of PM ϕ should be routinely monitored before EV production. Nevertheless, M2-EVs may be a promising multitarget nanomedicine to attenuate severe infection-related cytokine storms, such as recent COVID-19.

4. Conclusion

In summary, primary peritoneal M2 macrophages exhibited superior anti-inflammatory potential than immobilized cell lines in decreasing bacterial endotoxin-induced cytokine (e.g., TNF- α , IL-6) release. M2-EVs were able to decrease bacterial endotoxin-induced cytokine (e.g., TNF- α , IL-6) release and its associated oxidative stress and multiple organ damage, which might be mediated by inhibiting multiple key proinflammatory pathways (e.g., NF- κ B, JAK-STAT, p38 MAPK) by delivering a set of functional cargos and regulating complex miRNA-gene/gene networks, which is different from the existing single cytokine-targeted therapy. In addition, human peritoneal M2-EVs were able to exert as anti-inflammatory agents and serve as nanodecoys to prevent SARS-CoV-2 pseudovirus infection *in vitro* due to their surface angiotensin-converting enzyme 2 (ACE2), a receptor of the SARS-CoV-2 spike protein.

Author contributions

Jingping Liu and Yizhuo Wang designed the project. Jingping Liu, Yizhuo Wang, Shuyun Liu, Peng Lou, Meng Zhao, Lan Li, Ke Lv, Yujia Yuan and Meihua Wan performed the experiments, collected the data, and analyzed and interpreted the data. Ling Li and Xueli Zhou collected the patient peritoneal dialysate samples. All authors contributed to the writing of the manuscript, discussed the results and implications, and edited the manuscript at all stages.

Declaration of Competing Interest

The authors declare that they have no known competing financial interests or personal relationships that could have appeared to influence the work reported in this paper.

Acknowledgments

This work was partly supported by the National Natural Science Foundation of China (32071453, 31871001, 81571808, 81774160), Health Commission of Sichuan Province (20PJ003), and 1.3.5 Project for Disciplines of Excellence (ZYG18014), West China Hospital of

Sichuan University. The authors would like to thank Sichuan Neo-life Stem Cell Biotech & Sichuan Stem Cell Bank for providing the hMSCs, Jie Zhang and Lin Bai for providing technical assistance with confocal microscopy, and Shisheng Wang for providing technical assistance with the bioinformatics analysis.

Appendix A. Supplementary data

Supplementary data to this article can be found online at <https://doi.org/10.1016/j.jconrel.2022.06.063>.

References

- [1] B. Allegranzi, S. Bagheri Nejad, C. Combesure, W. Graafmans, H. Attar, L. Donaldson, D. Pittet, Burden of endemic health-care-associated infection in developing countries: systematic review and meta-analysis, *Lancet* 377 (9761) (2011) 228–241.
- [2] A. Gharamti, O. Samara, A. Monzon, S. Scherger, K. DeSanto, S. Sillau, C. Franco-Paredes, A. Henao-Martinez, L. Shapiro, Association between cytokine levels, sepsis severity and clinical outcomes in sepsis: a quantitative systematic review protocol, *BMJ Open* 11 (8) (2021), e048476.
- [3] R. Karki, T.D. Kanneganti, The 'cytokine storm': molecular mechanisms and therapeutic prospects, *Trends Immunol.* 42 (8) (2021) 681–705.
- [4] F. Coperchini, L. Chiovato, L. Croce, F. Magri, M. Rotondi, The cytokine storm in COVID-19: An overview of the involvement of the chemokine/chemokine-receptor system, *Cytokine Growth Factor Rev.* 53 (2020) 25–32.
- [5] C. Huang, Y. Wang, X. Li, L. Ren, J. Zhao, Y. Hu, L. Zhang, G. Fan, J. Xu, X. Gu, Z. Cheng, T. Yu, J. Xia, Y. Wei, W. Wu, X. Xie, W. Yin, H. Li, M. Liu, Y. Xiao, H. Gao, L. Guo, J. Xie, G. Wang, R. Jiang, C. U. Louis, N. Ahmed, M. Jensen, S.A. Grupp, C. L. Mackall, Current concepts in the diagnosis and management of cytokine release syndrome, *Blood* 124 (2) (2014) 188–195.
- [6] Y. Guo, T. Li, X. Xia, B. Su, H. Li, Y. Feng, J. Han, X. Wang, L. Jia, Z. Bao, J. Li, Y. Liu, L. Li, Different profiles of antibodies and cytokines were found between severe and moderate COVID-19 patients, *Front. Immunol.* 12 (2021), 723585.
- [7] Q.F. Meng, R. Tian, H. Long, X. Wu, J. Lai, O. Zharkova, J.W. Wang, X. Chen, L. Rao, Capturing cytokines with advanced materials: a potential strategy to tackle COVID-19 cytokine storm, *Adv. Mater.* 33 (20) (2021), e2100012.
- [8] D.W. Lee, R. Gardner, D.L. Porter, C.U. Louis, N. Ahmed, M. Jensen, S.A. Grupp, C. L. Mackall, Current concepts in the diagnosis and management of cytokine release syndrome, *Blood* 124 (2) (2014) 188–195.
- [9] W. Zhang, Y. Zhao, F. Zhang, Q. Wang, T. Li, Z. Liu, J. Wang, Y. Qin, X. Zhang, X. Yan, X. Zeng, S. Zhang, The use of anti-inflammatory drugs in the treatment of people with severe coronavirus disease 2019 (COVID-19): The Perspectives of clinical immunologists from China, *Clin. Immunol.* 214 (2020), 108393.
- [10] Y. Wang, M. Zhao, S. Liu, J. Guo, Y. Lu, J. Cheng, J. Liu, Macrophage-derived extracellular vesicles: diverse mediators of pathology and therapeutics in multiple diseases, *Cell Death Dis.* 11 (10) (2020) 924.
- [11] S.J. Carter, R.S. Tattersall, A.V. Ramanan, Macrophage activation syndrome in adults: recent advances in pathophysiology, diagnosis and treatment, *Rheumatology (Oxford)* 58 (1) (2019) 5–17.
- [12] Y. Lin, X. Yang, W. Yue, X. Xu, B. Li, L. Zou, R. He, Chemerin aggravates DSS-induced colitis by suppressing M2 macrophage polarization, *Cell. Mol. Immunol.* 11 (4) (2014) 355–366.
- [13] P. Lou, S. Liu, X. Xu, C. Pan, Y. Lu, J. Liu, Extracellular vesicle-based therapeutics for the regeneration of chronic wounds: current knowledge and future perspectives, *Acta Biomater.* 119 (2021) 42–56.
- [14] R. Yang, Y. Liao, L. Wang, P. He, Y. Hu, D. Yuan, Z. Wu, X. Sun, Exosomes derived from M2b macrophages attenuate DSS-induced colitis, *Front. Immunol.* 10 (2019) 2346.
- [15] C.P. Dang, A. Leelahavanichkul, Over-expression of miR-223 induces M2 macrophage through glycolysis alteration and attenuates LPS-induced sepsis mouse model, the cell-based therapy in sepsis, *PLoS One* 15 (7) (2020), e0236038.
- [16] R. Mao, C. Wang, F. Zhang, M. Zhao, S. Liu, G. Liao, L. Li, Y. Chen, J. Cheng, J. Liu, Y. Lu, Peritoneal M2 macrophage transplantation as a potential cell therapy for enhancing renal repair in acute kidney injury, *J. Cell. Mol. Med.* 24 (6) (2020) 3314–3327.
- [17] Q. Cao, Y. Wang, C. Wang, X.M. Wang, V.W.S. Lee, G. Zheng, Y. Zhao, S. I. Alexander, D.C.H. Harris, Therapeutic potential of regulatory macrophages generated from peritoneal dialysate in adriamycin nephropathy, *Am. J. Physiol. Ren. Physiol.* 314 (4) (2018) F561–F571.
- [18] M. Zhao, S. Liu, C. Wang, Y. Wang, M. Wan, F. Liu, M. Gong, Y. Yuan, Y. Chen, J. Cheng, Y. Lu, J. Liu, Mesenchymal stem cell-derived extracellular vesicles attenuate mitochondrial damage and inflammation by stabilizing mitochondrial DNA, *ACS Nano* 15 (1) (2021) 1519–1538.
- [19] J. Webber, A. Clayton, How pure are your vesicles? *J Extracell Vesicles* 2 (2013).
- [20] L. Chang, G. Zhou, O. Soufan, J. Xia, miRNet 2.0: network-based visual analytics for miRNA functional analysis and systems biology, *Nucleic Acids Res.* 48 (W1) (2020) W244–W251.
- [21] L. Chen, R. Chen, S. Kemper, M. Cong, H. You, D.R. Brigstock, Therapeutic effects of serum extracellular vesicles in liver fibrosis, *J Extracell Vesicles* 7 (1) (2018) 1461505.

- [22] C. Wang, S. Wang, Y. Chen, J. Zhao, S. Han, G. Zhao, J. Kang, Y. Liu, L. Wang, X. Wang, Y. Xu, S. Wang, Y. Huang, J. Wang, J. Zhao, Membrane nanoparticles derived from ACE2-rich cells block SARS-CoV-2 infection, *ACS Nano* 15 (4) (2021) 6340–6351.
- [23] F. Coccozza, N. Nevo, E. Piovesana, X. Lahaye, J. Buchrieser, O. Schwartz, N. Manel, M. Tkach, C. Thery, L. Martin-Jaular, Extracellular vesicles containing ACE2 efficiently prevent infection by SARS-CoV-2 Spike protein-containing virus, *J Extracell Vesicles* 10 (2) (2020), e12050.
- [24] J. Wang, P. Kubes, A reservoir of mature cavity macrophages that can rapidly invade visceral organs to affect tissue repair, *Cell* 165 (3) (2016) 668–678.
- [25] M.K. Neog, F. Sultana, M. Rasool, Targeting RAW 264.7 macrophages (M1 type) with Withaferin-A decorated mannoseylated liposomes induces repolarization via downregulation of NF-kappaB and controlled elevation of STAT-3, *Int. Immunopharmacol.* 61 (2018) 64–73.
- [26] J.M. Cavaillon, Exotoxins and endotoxins: inducers of inflammatory cytokines, *Toxicol* 149 (2018) 45–53.
- [27] A. Yoshimura, Y. Wakabayashi, T. Mori, Cellular and molecular basis for the regulation of inflammation by TGF-beta, *J. Biochem.* 147 (6) (2010) 781–792.
- [28] T. Imai, Y. Takahashi, M. Nishikawa, K. Kato, M. Morishita, T. Yamashita, A. Matsumoto, C. Charoenviriyakul, Y. Takakura, Macrophage-dependent clearance of systemically administered B16BL6-derived exosomes from the blood circulation in mice, *J Extracell Vesicles* 4 (2015) 26238.
- [29] L.A. Mulcahy, R.C. Pink, D.R. Carter, Routes and mechanisms of extracellular vesicle uptake, *J Extracell Vesicles* 3 (2014).
- [30] C. Escrevente, S. Keller, P. Altevogt, J. Costa, Interaction and uptake of exosomes by ovarian cancer cells, *BMC Cancer* 11 (2011) 108.
- [31] D. Cox, C.C. Tseng, G. Bjekic, S. Greenberg, A requirement for phosphatidylinositol 3-kinase in pseudopod extension, *J. Biol. Chem.* 274 (3) (1999) 1240–1247.
- [32] P. Wu, B. Zhang, H. Shi, H. Qian, W. Xu, MSC-exosome: a novel cell-free therapy for cutaneous regeneration, *Cytotherapy* 20 (3) (2018) 291–301.
- [33] B.C. Lee, I. Kang, K.R. Yu, Therapeutic features and updated clinical trials of mesenchymal stem cell (MSC)-derived exosomes, *J. Clin. Med.* 10 (4) (2021).
- [34] J.S. Kim, J.Y. Lee, J.W. Yang, K.H. Lee, M. Effenberger, W. Szpirt, A. Kronbichler, J. I. Shin, Immunopathogenesis and treatment of cytokine storm in COVID-19, *Theranostics* 11 (1) (2021) 316–329.
- [35] L. Faulkner, A. Cooper, C. Fantino, D.M. Altmann, S. Sriskandan, The mechanism of superantigen-mediated toxic shock: not a simple Th1 cytokine storm, *J. Immunol.* 175 (10) (2005) 6870–6877.
- [36] M.P. Fink, S.O. Heard, Laboratory models of sepsis and septic shock, *J. Surg. Res.* 49 (2) (1990) 186–196.
- [37] S. Peerapornratana, C.L. Manrique-Caballero, H. Gomez, J.A. Kellum, Acute kidney injury from sepsis: current concepts, epidemiology, pathophysiology, prevention and treatment, *Kidney Int.* 96 (5) (2019) 1083–1099.
- [38] C. Manickam, S.V. Shah, O. Lucar, D.R. Ram, R.K. Reeves, Cytokine-mediated tissue injury in Non-human primate models of viral infections, *Front. Immunol.* 9 (2018) 2862.
- [39] M. Zhao, Y. Wang, L. Li, S. Liu, C. Wang, Y. Yuan, G. Yang, Y. Chen, J. Cheng, Y. Lu, J. Liu, Mitochondrial ROS promote mitochondrial dysfunction and inflammation in ischemic acute kidney injury by disrupting TFAM-mediated mtDNA maintenance, *Theranostics* 11 (4) (2021) 1845–1863.
- [40] Y.C. Chen, H.C. Sung, T.Y. Chuang, T.C. Lai, T.L. Lee, C.W. Lee, I.T. Lee, Y.L. Chen, Vitamin D3 decreases TNF-alpha-induced inflammation in lung epithelial cells through a reduction in mitochondrial fission and mitophagy, *Cell Biol. Toxicol.* 38 (2021) 427–450.
- [41] X. Yan, D. Zeng, H. Zhu, Y. Zhang, Y. Shi, Y. Wu, H. Tang, D. Li, miRNA-532-5p regulates CUMS-induced depression-like behaviors and modulates LPS-induced proinflammatory cytokine signaling by targeting STAT3, *Neuropsychiatr. Dis. Treat.* 16 (2020) 2753–2764.
- [42] K. Dubois-Camacho, D. Diaz-Jimenez, M. De la Fuente, R. Quera, D. Simian, M. Martinez, G. Landskron, M. Olivares-Morales, J.A. Cidlowski, X. Xu, G. Gao, J. Xie, J. Chnaiderman, R. Soto-Rifo, M.J. Gonzalez, A. Calixto, M.A. Hermoso, Inhibition of miR-378a-3p by inflammation enhances IL-33 levels: a novel mechanism of alarmin modulation in ulcerative colitis, *Front. Immunol.* 10 (2019) 2449.
- [43] Y. Wei, M. Nazari-Jahantigh, L. Chan, M. Zhu, K. Heyll, J. Corbalan-Campos, P. Hartmann, A. Thiemann, C. Weber, A. Schober, The microRNA-342-5p fosters inflammatory macrophage activation through an Akt1- and microRNA-155-dependent pathway during atherosclerosis, *Circulation* 127 (15) (2013) 1609–1619.
- [44] J. Rong, L. Xu, Y. Hu, F. Liu, Y. Yu, H. Guo, X. Ni, Y. Huang, L. Zhao, Z. Wang, Inhibition of let-7b-5p contributes to an anti-tumorigenic macrophage phenotype through the SOCS1/STAT pathway in prostate cancer, *Cancer Cell Int.* 20 (2020) 470.
- [45] Nature's second pandemic progress report, *Nature* 586 (7830) (2020) 473–474.
- [46] K. Lim, G. Nishide, T. Yoshida, T. Watanabe-Nakayama, A. Kobayashi, M. Hazawa, R. Hanayama, T. Ando, R.W. Wong, Millisecond dynamic of SARS-CoV-2 spike and its interaction with ACE2 receptor and small extracellular vesicles, *J Extracell Vesicles* 10 (14) (2021), e12170.
- [47] F. Xie, P. Su, T. Pan, X. Zhou, H. Li, H. Huang, A. Wang, F. Wang, J. Huang, H. Yan, L. Zeng, L. Zhang, F. Zhou, Engineering extracellular vesicles enriched with palmitoylated ACE2 as COVID-19 therapy, *Adv. Mater.* 33 (49) (2021), e2103471.
- [48] J. Lv, Z. Wang, Y. Qu, H. Zhu, Q. Zhu, W. Tong, L. Bao, Q. Lv, J. Cong, D. Li, W. Deng, P. Yu, J. Song, W.M. Tong, J. Liu, Y. Liu, C. Qin, B. Huang, Distinct uptake, amplification, and release of SARS-CoV-2 by M1 and M2 alveolar macrophages, *Cell Discov* 7 (1) (2021) 24.
- [49] Z. Leng, R. Zhu, W. Hou, Y. Feng, Y. Yang, Q. Han, G. Shan, F. Meng, D. Du, S. Wang, J. Fan, W. Wang, L. Deng, H. Shi, H. Li, Z. Hu, F. Zhang, J. Gao, H. Liu, X. Li, Y. Zhao, K. Yin, X. He, Z. Gao, Y. Wang, B. Yang, R. Jin, I. Stambler, L.W. Lim, H. Su, A. Moskalev, A. Cano, S. Chakrabarti, K.J. Min, G. Ellison-Hughes, C. Caruso, K. Jin, R.C. Zhao, Transplantation of ACE2(-) Mesenchymal Stem Cells Improves the Outcome of Patients with COVID-19 Pneumonia, *Aging Dis.* 11 (2) (2020) 216–228.
- [50] D. Sharma, F. Zhao, Updates on clinical trials evaluating the regenerative potential of allogenic mesenchymal stem cells in COVID-19, *NPJ Regen Med* 6 (1) (2021) 37.
- [51] T. Coccini, A. Spinillo, M. Rocco, E. Lenta, C. Valsecchi, U. De Simone, Human umbilical cord mesenchymal stem cell-based in vitro model for neurotoxicity testing, *Curr Protoc* 2 (4) (2022), e423.
- [52] W. Pei, X. Li, R. Bi, X. Zhang, M. Zhong, H. Yang, Y. Zhang, K. Lv, Exosome membrane-modified M2 macrophages targeted nanomedicine: treatment for allergic asthma, *J. Control. Release* 338 (2021) 253–267.